

Obstacle Avoidance Deep Reinforcement Learning-Based Trajectory Planner with Robust Low-Level Control for Robotic Manipulators*

Mehdi Heydari Shahna, Seyed Adel Alizadeh Kolagar, and Jouni Mattila

Abstract—In robotics, contemporary strategies are learning-based, characterized by a complex black-box nature and a lack of interpretability, which may pose challenges in ensuring stability and safety. To address these issues, we propose integrating an obstacle-free deep reinforcement learning (DRL) trajectory planner with a novel auto-tuning low- and joint-level control strategy, all while actively engaging in the learning phase through interactions with the environment. This approach circumvents the complexities associated with computations while also addressing nonrepetitive and random obstacle avoidance tasks. First, a model-free DRL agent to plan velocity-bounded and obstacle-free motion is employed for a manipulator with ‘n’ degrees of freedom (DoF) in task space through joint-level reasoning. This plan is then input into a robust subsystem-based adaptive controller, which produces the necessary torques, while the Cuckoo Search Optimization (CSO) algorithm enhances control gains to minimize the time required to reach, time taken to stabilize, the maximum deviation from the desired value, and persistent tracking error in the steady state. This approach guarantees that position and velocity errors exponentially converge to zero in an unfamiliar environment, despite unknown robotic manipulator modeling. Theoretical assertions are validated through the presentation of simulation outcomes.

Index Terms—Robust control, robotic manipulator, deep reinforcement learning.

I. INTRODUCTION

Robot control involves three levels of abstraction: motor, motion, and task levels [1]. For instance, tasks involving the tracking of predefined joint trajectories primarily fall under motor-level control. However, a more comprehensive approach is necessary for goal-reaching tasks, one involving both motion planning and motor control. Finally, complex tasks, such as welding and polishing require the integration of all three control levels. Autonomous robot systems rely heavily on motion planning to tackle the challenge of determining a viable, seamless, and obstacle-free route within a robot’s configuration space from an initial to a target point [2], [3]. This identified path can then be followed by a low-level controller [4]. Motion planning commonly employs either sampling-based approaches [5] or optimization-based methods [6]. The former of which guarantees a globally optimum infinite compute time, demonstrating completeness [5]. However, in practice, they often exhibit sample inefficiency and have the propensity to generate non-smooth trajectories [7]. Conversely, optimization-based planners refine initial

*Funding for this research was provided by the Business Finland partnership project “Future All-Electric Rough Terrain Autonomous Mobile Manipulators” (Grant No. 2334/31/2022).

All authors are with Faculty of Engineering and Natural Sciences, Tampere University, Finland {firstname.lastname}@tuni.fi

trajectories through preconditioned gradient descent [6] or stochastic update rules [8], allowing the incorporation of such desired properties as smoothness into optimized costs. However, planners based on optimization rely on proficient initialization and may become ensnared in local minima owing to the non-convex characteristics of intricate problems.

As a current focal point of interest, learning-based methods have gained widespread use for addressing intricate challenges in path and trajectory planning [9]. Specifically, reinforcement learning (RL) stands out as an exemplary machine learning paradigm, as its algorithms inherently acquire knowledge through direct interactions with the environment [10]. As shown in Fig. 1, in the RL, an agent engages with the environment, encounters diverse situations, and receives rewards. By harnessing this experiential knowledge, agents can acquire the ability to make the best decisions in each state [11]. Traditional RL is constrained to domains featuring uncomplicated state representations, so to overcome challenges presented by higher-dimensional and more intricate problems, the integration of deep neural networks (DNNs) into RL has given rise to the paradigm known as Deep Reinforcement Learning (DRL) [12], which has shown promising results in the field of robot navigation with continuous action and state space. DRL algorithms can be classified into two principal types: model-based and model-free methods. For motion planning, model-free DRL algorithms hold prominence, given the intricacies involved in modeling a dynamic environment [13]. Model-free algorithms encompass policy-based, value-based (DQN-based), and actor-critic methods, the latter combining advantages from both policy and value-based approaches. Nevertheless, DQN-based methods face limitations in addressing problems characterized by discrete and lower-dimensional action spaces as well as deterministic policies. Simultaneously, policy gradient approaches demonstrate versatility by accommodating continuous action spaces and the representation of stochastic policies. A sample-efficient strategy involves employing an actor-critic architecture capable of effectively utilizing off-policy data [14]. Because Soft Actor-Critic-based (SAC) algorithms use an entropy term in their objective function, they can find the optimal solution to the high-dimensional problem, suggesting that the SAC-based algorithm outperformed the existing results [15].

Recent trends in robotics favor embedding established control principles, such as PD-controlled joint positions [16], or impedance control [17] into the action space, diverging from earlier end-to-end policies that directly output low-level control commands, such as joint torques [18], [19].

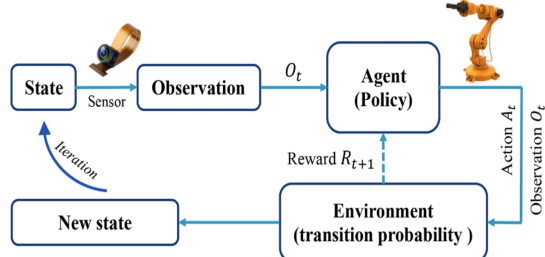


Fig. 1: The architecture of RL-based learning [1].

This shift simplifies learning by outputting higher-level policy control commands, such as reference joint velocities, which are subsequently processed by low-level controllers. However, learning policies concerning this joint torque action space can be complex, as they need to grasp the intricacies of the robot's kinematics and dynamics, especially because rewards are typically expressed using task space properties [20]. In addition, despite considerable advancements in learning-based joint-level control, it seldom achieves exponentially fast convergence to the reference trajectories, a factor prominent in ensuring control stability and fast goal achievement. This form of stability is capable of enhancing the interpretability of overall robot motions and generalizes learned policies to handle a broader range of situations and variations. Furthermore, achieving optimal results through this control application may necessitate meticulous parameter tuning. Striking the proper balance between performance aspects can be challenging in unknown environments [21], especially considering that the overall performance of the control structure depends on the low-level control's ability to respond quickly and effectively to the learning-based motion planner. Metaheuristic algorithms, often inspired by nature, have become widely adopted tools for optimization due to their straightforward application and low computational demands, currently among the most extensively used algorithms [22]. Unlike Genetic Algorithms (GAs), CSO stands out with a single specific parameter, streamlining the focus on general parameter selection. This distinctive feature makes CSO particularly suitable for perfecting control gains. As such, investigations indicated that CSO exhibits the capacity to demonstrate considerably greater efficiency than Particle Swarm Optimization (PSO), GAs, and Artificial Bee Colony (ABC) [23]–[25].

To enhance the control performance of goal-reaching tasks for a manipulator with 'n' degrees of freedom (DoF), this paper introduces a novel, robust, joint-level control strategy to perform nonrepetitive tasks by utilizing a velocity-bounded, model-free DRL agent for obstacle-free motion planning. We train the DRL agent in conjunction with a model-free low-level control section within the closed-loop system, enabling it to compensate for uncertainties arising from the integration of the DRL agent and the controller section, ensuring exponential convergence of tracking errors to zero. Simultaneously, optimal gains are adjusted using CSO tailored to minimize time-domain criteria. In summary,

this study makes notable contributions to the field of robot control, as follows: (1) all components of the strategy, involving the integration of an obstacle-free DRL-based trajectory planner with a novel auto-tuning low- and joint-level control strategy, actively participate in the learning phase through interactions with the unknown environment. This approach significantly reduces computational demands when compared to methods relying solely on continuous DRL control action; (2) this incorporation compensates for uncertainties arising from the integration of the DRL agent and the low-level controller in uniformly exponential stability; (3) and by considering time-domain criteria, optimal control gains are achieved.

The subsequent sections of the article are structured in the following manner: Section II presents the modeling of the system and defines the problem components of n-DoF manipulators. Section III introduces the DRL motion planning architecture. Section IV presents the robust low-level control design by utilizing an adaptive subsystem-based strategy, optimizing the controller gains by customizing CSO, as well as presents the stability analysis. In Section V, the proposed control strategy is validated by developing the manipulator system provided in [26] in consideration of obstacles in nonrepetitive tasks.

II. MODELING AN N-DOF ROBOTIC MANIPULATOR SYSTEM

The dynamic model for an n-DoF robotic manipulator is provided, as follows [27]:

$$M(q)\ddot{q} = \tau - C_m(q, \dot{q})\dot{q} - f(\dot{q}) - G(q) - \tau_L \quad (1)$$

where $q \in \mathbb{R}^n$ represents the joint angles. The mapping $M(q) : \mathbb{R}^n \rightarrow \mathbb{R}^{n \times n}$ describes the inertia properties, where $C_m(q, \dot{q}) : \mathbb{R}^n \times \mathbb{R}^n \rightarrow \mathbb{R}^{n \times n}$ accounts for the centrifugal and Coriolis forces. The function $G(q) : \mathbb{R}^n \rightarrow \mathbb{R}^n$ computes the gravitational torques, whereas the function $f(\dot{q}) : \mathbb{R}^n \rightarrow \mathbb{R}^n$ represents the resistance to movement. The vector $\tau \in \mathbb{R}^n$ includes torques applied at the joints, and $\tau_L \in \mathbb{R}^n$ characterizes external disturbances affecting the joints. To simplify the manipulator dynamics in the subsystem-based form, we transform (1), as follows:

$$\dot{q}_1(t) = q_2(t), \quad \dot{q}_2(t) = M^{-1}(q_1)\tau + F(q_1, q_2) + \tau_d(t) \quad (2)$$

where $q_1 = q = [q_1(1), q_1(2)]^\top$, and $q_2 = \dot{q} = [q_2(1), q_2(2)]^\top$ are the system states, and $F = -M^{-1}(C_m q_2 + f + G)$ and $\tau_d = -M^{-1}\tau_L$ can be uncertainties and load effects, respectively. In addition, the tracking errors are defined, as follows:

$$e_1 = q_1 - q_{1d}, \quad e_2 = q_2 - q_{2d} \quad (3)$$

where $q_{1d} \in \mathbb{R}^n$ and $\dot{q}_{1d} (= q_{2d}) \in \mathbb{R}^n$ are the desired position and velocity trajectories, respectively.

III. REINFORCEMENT LEARNING-BASED TRAJECTORY PLANNING

The objective of our DRL agent is to plan a motion for a robotic manipulator with 'n' DoFs in task space, ensuring both velocity constraints and collision-free trajectories with

joint-level commands. To achieve this goal, we adopted the SAC algorithm (see algorithm 1) [28], [29], recognized for its proficiency in solving complex tasks, as discussed in Section I. A crucial aspect of the successful learning of the agent involves a precise definition of states, actions, and rewards in the training process.

A. State and Action Representation

The majority of robotic systems based on RL acquire knowledge in the task space as opposed to the joint space [17], [30], [31]. Operating in the task space, specifically the Cartesian end-effector space, significantly simplifies the learning problem. Nevertheless, these solutions prove inadequate in unstructured environments where collisions between the robot and the surroundings necessitate joint-level reasoning. Furthermore, the majority of approaches rely on solving inverse kinematics or dynamics equations to translate the task space into joint space, primarily for collision avoidance [32]. The agent can output desired positions, velocities, accelerations, or torques, each of them has its own pros and cons. In our system, we chose the joint velocities as our actions due to their high performance in achieving tasks [20]. As such, we can constrain the velocities for each joint according to the motor properties or tip velocity. Goal-reaching tasks involve three progressively complex levels of motion planning. The initial level focuses on reaching the goal without encountering any obstacles. The second level addresses scenarios in which obstacles are present, requiring the end-effector to navigate while avoiding collisions. The third and most intricate level necessitates the manipulator to reach the goal amid obstacles, ensuring both the tip and links avoid collision with them. We selected states, actions, and rewards, drawing inspiration from [32] and [20]. In the first situation, the state s_t is defined as:

$$s_t = \langle p_t, \delta p_t, p, q_1 \rangle \quad (4)$$

Here, $p_t = (p_{tx}, p_{ty}, p_{tz})$ signifies the Cartesian position of the target. If access to the absolute target position is unavailable, this term can be omitted, although it complicates the training process. $\delta p_t = (\delta p_x, \delta p_y, \delta p_z)$ represents the end-effector error (distance between the tip and target), $p = (p_x, p_y, p_z)$ denotes the Cartesian position of the end effector, and $q_1 \in \mathbb{R}^n$ represents the values for the n joints of the manipulator.

In the second situation, the state can be adjusted to the following format.

$$s_t = \langle p_t, \delta p_t, p, q_1, \delta p_o \rangle \quad (5)$$

Here, $\delta p_o = (\delta p_{o1}, \dots, \delta p_{om})$ indicates the position error between the end-effector and each obstacle. Unlike δp_t , this considers the absolute distance between the tip and the obstacles, enabling the manipulator to function in an environment in which the obstacle's absolute position is unknown, necessitating reliance on relative positions obtained through sensors.

For the third situation, the state is defined as:

$$s_t = \langle p_t, \delta p_t, p, q_1, \delta p_o, \delta p_{ol} \rangle \quad (6)$$

Here, $\delta p_{ol} = (\delta p_{ol1}, \dots, \delta p_{olm})$ represents the minimum distance between each link and its nearest obstacle.

In all scenarios, the actions remain consistent, involving joint velocities:

$$a_t = \langle \dot{q}_{1d} \rangle = \langle q_{2d} \rangle \quad (7)$$

and $q_{2d} \in \mathbb{R}^n$ represents the desired joint velocities. These formulations ensure the states are appropriately modified to meet the specified requirements, while maintaining consistent actions.

B. Reward Function

Our reward function $r(s, a)$ is defined as follows:

$$r(s, a) = \begin{cases} \text{reach_reward} & \text{if the tip reaches the target} \\ -\text{boundary_penalty} & \text{if joint angles reach the limits} \\ -\text{obstacle_penalty} & \text{if there is a collision} \\ -\log_{10}(1 + \text{tip error} - \text{threshold}) & \text{otherwise} \\ (r(s, a) - 1) & (\text{if the tip error increases}) \end{cases} \quad (8)$$

The initial component constitutes a positive reward given to the agent upon successful attainment of the target. To ensure controlled movements within the specified workspace, limits are imposed on the manipulator. Should any joint angle exceed the predefined constraints, the agent faces a boundary penalty. In addition, collision occurrences, irrespective of type, result in an obstacle penalty. Alternatively, the reward is determined by a formula, where the tip error represents the absolute distance between the manipulator's tip and the target. The threshold, acting as the acceptable error limit for considering the goal achieved, is factored into this computation. To motivate expedited movements further, an added penalty is introduced. If the tip error increases after progressing to the next step, the agent incurs a “-1” penalty, encouraging the manipulator to accelerate its progress toward the target.

C. Learning Procedure

To begin the learning process, the environment is initially defined. In the context of our DRL algorithm, both the controller and manipulator model collectively form our environment. This implies the action generated by the agent enters a closed loop, encompassing both the controller and the model, following environment parameters. Subsequently, the workspace is established. This involves outlining the points accessible to the manipulator within the desired region. In addition, the positions of obstacles are specified, and points that are a certain distance from the obstacles are removed, enabling a collision-free workspace. Following the environmental setup, essential variables and functions for the DRL agent are assigned. These include the observation and action space, reset function, step time, and maximum episode time. Simulation resets and the beginning of a new episode occurs when a joint surpasses its limits, the manipulator attains its goal, a collision occurs, or the number of simulation steps exceeds the limit. Subsequently, the SAC agent is created using the provided information. Training is then initiated by configuring the training parameters accordingly.

Algorithm 1. Soft actor-critic Algorithm

Input: Initial parameters θ , ψ , and ϕ .
Output: Optimized parameters θ , ψ , and ϕ .

```

1 Initialize target network weights  $\bar{\theta} \leftarrow \theta$ ,  $\bar{\psi} \leftarrow \psi$ ;
2 Initialize an empty replay pool  $\mathcal{D} \leftarrow \emptyset$ ;
3 for each iteration do
4   Set the manipulator position to the defined initial state;
5   Randomly choose the target position from the collision-free workspace;
6   for each environment step do
7     Sample action from the policy  $\mathbf{a}_t \sim \pi_\phi(\mathbf{a}_t | \mathbf{s}_t)$ ;
8     Sample transition from the environment  $\mathbf{s}_{t+1} \sim p(\mathbf{s}_{t+1} | \mathbf{s}_t, \mathbf{a}_t)$ ;
9     (including giving action  $a_t = q_{2d}$  as input to algorithm 3 and waiting for the environment response)
10    Store the transition in the replay pool  $\mathcal{D} \leftarrow \mathcal{D} \cup \{(\mathbf{s}_t, \mathbf{a}_t, r(\mathbf{s}_t, \mathbf{a}_t), \mathbf{s}_{t+1})\}$ ;
11  end
12  for each gradient step do
13    Update value network weights  $\psi \leftarrow \psi - \lambda_v \hat{\nabla}_\psi J_v(\psi)$ ;
14     $J_v(\psi) = \mathbb{E}_{\mathbf{s}_t \sim \mathcal{D}} \left[ \frac{1}{2} \left( V_\psi(\mathbf{s}_t) - \mathbb{E}_{\mathbf{a}_t \sim \pi_\phi} [Q_\theta(\mathbf{s}_t, \mathbf{a}_t) - \log \pi_\phi(\mathbf{a}_t | \mathbf{s}_t)] \right)^2 \right]$ ;
15    Update the Q-function parameters  $\theta_i \leftarrow \theta_i - \lambda_Q \hat{\nabla}_{\theta_i} J_Q(\theta_i)$  for  $i \in \{1, 2\}$ ;
16     $J_Q(\theta) = \mathbb{E}_{(\mathbf{s}_t, \mathbf{a}_t) \sim \mathcal{D}} \left[ \frac{1}{2} (Q_\theta(\mathbf{s}_t, \mathbf{a}_t) - r(\mathbf{s}_t, \mathbf{a}_t) - \gamma \mathbb{E}_{\mathbf{s}_{t+1} \sim p} [V_\psi(\mathbf{s}_{t+1})])^2 \right]$ ;
17    Update policy weights  $\phi \leftarrow \phi - \lambda_\pi \hat{\nabla}_\phi J_\pi(\phi)$ ;
18     $J_\pi(\phi) = \mathbb{E}_{\mathbf{s}_t \sim \mathcal{D}, \mathbf{e}_t \sim \mathcal{N}} [\log \pi_\phi(f_\phi(\mathbf{e}_t; \mathbf{s}_t) | \mathbf{s}_t) - Q_\theta(\mathbf{s}_t, f_\phi(\mathbf{e}_t; \mathbf{s}_t))]$ ;
19    Substitute target network weights  $\bar{\psi} \leftarrow \tau \psi + (1 - \tau) \bar{\psi}$ ;
20  end
21 end

```

IV. ROBUST DRL-BASED CONTROL STRUCTURE

A. Cuckoo Search Optimization

The CSO mimics cuckoos' brood parasitism, optimizing by selecting nests with optimal solutions through a random walk with a power-law step-length distribution [22]. Similar to [25], this paper concentrates on minimizing the objective function of a low-level controller that includes time-domain features, such as the overshoot, rise time, settling time, and steady state of the tracking error of the trajectories commanded by Section III. We assume the number of cuckoo eggs (control gains) is defined as ζ , deposited in a randomly chosen nest $B_j \in \mathbb{R}^{1 \times \zeta}$ for $j = 1, \dots, \eta$ in which η is the swarm (population) size. The best nest $B_{best} \in \mathbb{R}^{1 \times \zeta}$, housing optimal solutions, are retained for the next generation of cuckoos, and new nests for cuckoos are generated using a global random walk called Lévy flights with a specific iteration ($= n_{iteration}$), expressed as follows:

$$B_{j(new)} = B_j + \ell \cdot \text{levy}(stp) \quad (9)$$

where $B_{j(new)}$ and B_j are new and current nest, respectively. The parameter ℓ is a random number normally distributed, considering the scale of the problem at hand, and the change in position during the flight is considered as follows:

$$\text{levy}(stp) = 0.01 \cdot stp \cdot (B_j - B_{best}) \quad (10)$$

where stp represents a random step and is generated by a symmetric levy distribution [33], as:

$$stp = \frac{u}{|Y|^{\frac{1}{\beta}}} \quad (11)$$

where, generally, $\beta = 1.5$, and by taking advantage of the $\Gamma(\cdot)$ distribution, we can say:

$$u = \ell \cdot \left(\frac{\Gamma(\beta + 1) \cdot \sin\left(\frac{\pi\beta}{2}\right)}{\Gamma\left(\frac{\beta + 1}{2}\right) \cdot \beta \cdot 2^{(\beta - 1)/2}} \right)^{\frac{1}{\beta}}, \quad Y = \ell \quad (12)$$

The Lévy flight process represents a prominent feature of a cuckoo search, facilitating the generation of new candidate solutions or eggs through a random walk [34], [35]. Then, current nests B_j are replaced with the new generation of nests B_{new} if they have a better objective function value. Otherwise, they do not change. Next, the available host nests are limited in number, and a host bird can detect the worst foreign eggs with a probability ($P_a\%$) and should be updated with new ones:

$$B_{j(new)} = B_j + \text{rand}(0, 1) \cdot (B_i - B_o) \quad (13)$$

if the new candidate has better fitness, as the final step of the first iteration. $i \in j$ and $o \in j$ are random integers from 1 to η . In summary, the steps involved in designing the optimal solution in this paper are outlined as Algorithm 2.

Algorithm 2. Cuckoo search optimization

Output: B_j and $B_{best} \in \mathbb{R}^{1 \times \zeta}$.

```

1 Define an objective function as [25];
2 Initialize candidates  $B_j \in \mathbb{R}^{1 \times \zeta}$  for  $j = 1, \dots, \eta$ ;
3 Evaluate the objective function value for each  $B_j$ ;
4 While iteration  $\leq n_{iteration}$ :
5   Find the best candidate  $B_{best}$ ;
6   Generate new candidates  $B_{j(new)}$  using Eq. (9);
7   Find the objective function value for each  $B_{j(new)}$ ;
8   Store the better candidates, as  $B_j$ , between  $B_{j(new)}$  and  $B_j$ ;
9   Discard  $P_a\%$  of the worst candidates;
10  Update them by new candidates  $B_{j(new)}$  using Eq. (13);
11  Find the objective function value for each  $B_{j(new)}$ ;
12  Store the better candidates, as  $B_j$ , between  $B_{j(new)}$  and  $B_j$ ;
13 end
14 Find the best candidate  $B_{best}$ ;
15 Display  $B_{best}$ 

```

B. Adaptive subsystem-based control

By considering the obstacle-free velocity-bounded trajectories obtained from Section III and (3), a new transformation of the tracking model is considered, as follows:

$$\Upsilon_1 = e_1, \quad \Upsilon_2 = e_2 - \tau_0 \quad (14)$$

The virtual control term, denoted by $\tau_0 \in \mathbb{R}^n$, to control joint positions by considering the reference velocities, is defined as follows:

$$\tau_0 = -\frac{1}{2}a_0\Upsilon_1 \quad (15)$$

Here, a_0 is a positive constant. If we define $q_d = [q_{1d}, q_{2d}]^\top$, we can express the derivative of (14) as follows:

$$\dot{\Upsilon}_1 = \Upsilon_2 + \tau_0, \quad \dot{\Upsilon}_2 = M^{-1}\tau + F^* + \tau_d - \ddot{q}_d \quad (16)$$

where \ddot{q}_d denotes the desired joint acceleration and is assumed bounded. According to (14) and (16), and by considering the derivative of τ_0 as a term of uncertainty, F^* is defined as follows:

$$F^* = F(q, \dot{q}) - \frac{\partial \tau_0}{\partial \Upsilon_1} \frac{d\Upsilon_1}{dt} \quad (17)$$

where we presume the function τ_0 is bounded and differentiable.

Assumption 1: Let m , τ_{\max} , and $A_{\max} \in \mathbb{R}^+$ be positive constants, and let $H : \mathbb{R}^n \rightarrow \mathbb{R}^+$ be a continuously bounded function with strictly positive values if the following condition is satisfied:

$$\|F^*\| \leq mH, \quad \|\tau_d\| \leq \tau_{\max}, \quad \|\ddot{q}_d\| \leq A_{\max} \quad (18)$$

where $\|\cdot\|$ is the Euclidean norm.

Definition 1 [36]: For $t \geq t_0$, the system tracking error $e = [e_1, e_2]^\top$ is uniformly exponentially stable if the following condition is satisfied:

$$\|e\| = \|\bar{q} - q_d\| \leq \bar{\alpha}e^{-\alpha(t-t_0)}\|\bar{q}(t_0)\| + \alpha^* \quad (19)$$

where $\bar{\alpha}, \alpha^*$, and $\alpha \in \mathbb{R}^+$ are positive constants. $\bar{q} = [q_1, q_2]^\top$ is any state vector of a robotic manipulator, and $q_d = [q_{1d}, q_{2d}]^\top$ is the reference vector. More precisely, e is uniformly exponentially stabilized within a defined region $\Psi(\tau)$ with radius R , as follows:

$$\Psi(R) := \{e \mid \|e\| \leq R = \alpha^*\} \quad (20)$$

The actual torque control τ is proposed, as follows:

$$\tau = \frac{-1}{2}M(a_1 + b_1\hat{\chi})\Upsilon_2 - M\Upsilon_1 \quad (21)$$

where a_1 , and b_1 are positive constants, and $\hat{\chi}$ is the adaptive law for the second subsystem and is defined as follows:

$$\dot{\hat{\chi}} = -c_1r_1\hat{\chi} + \frac{1}{2}b_1c_1\|\Upsilon_2\|^2 \quad (22)$$

where c_1 , c_2 , and r_1 are positive constants.

Assumption 2 [36]: According to the general solution of the given linear first-order ordinary differential equation in (22), by choosing an initial condition $\hat{\chi}(0) \geq 0$ for the system and knowing that the adaptive gains are positive, we can claim that for all $t \geq 0$, we can guarantee $\hat{\chi} \geq 0$.

By assuming the vector of the adaptive law error is $\tilde{\chi} = \hat{\chi} - \chi^*$, where $\hat{\chi}$ is used to estimate an unknown and constant parameter χ^* , we can obtain:

$$\dot{\tilde{\chi}} = -c_1r_1\tilde{\chi} + \frac{1}{2}b_1c_1\|\Upsilon_2\|^2 - c_1r_1\chi^* \quad (23)$$

where χ^* is defined, as follows:

$$\chi^* = b_1^{-1}(\mu m^2 + v_1 \tau_{\max}^2 + v_2 A_{\max}^2) \quad (24)$$

where μ , v_1 , and v_2 are positive constant. In summary, the steps for designing the subsystem-based controller and the schematic of the entire proposed system structure in this paper are outlined in Algorithm 3 and Figure 2, respectively.

Algorithm 3. Auto-tuning subsystem-based adaptive control strategy

Input: robot states from sensors, optimized q_{2d} (**algorithm 1**).

Output: control input τ .

```

1  While new action is provided: (from step 8 of algorithm 1)
2     $[a_0, a_1, b_1, c_1, r_1] = B_j$  (from algorithm 2);
3     $e_1 = q_1 - q_{1d}$ ;
4     $e_2 = q_2 - q_{2d}$ ;
5     $\Upsilon_1 = e_1$ ;
6     $\tau_0 = -\frac{1}{2}a_0\Upsilon_1$ ;
7     $\Upsilon_2 = e_2 - \tau_0$ ;
8     $\hat{\chi} = -c_1r_1\hat{\chi} + \frac{1}{2}b_1c_1\|\Upsilon_2\|^2$ ;
9     $\tau = -\frac{1}{2}(a_1 + b_1\hat{\chi})\Upsilon_2 - \Upsilon_1$ ;
9    Display  $\tau$ ;
10   end

```

C. Stability analysis

Theorem 1 Consider the manipulator system outlined in (2), which employs the control strategy specified in (15) and (21) along with the adaptive law in (22). For any positive control gains optimized by COA, the tracking errors between the actual states and the reference trajectories generated by the DRL-based motion planner provided in Section III converge to zero with uniformly exponential stability.

Proof: A Lyapunov function is suggested as follows:

$$V_1 = \frac{1}{2}[\Upsilon_1^\top \Upsilon_1] \quad (25)$$

After differentiating V_1 and inserting (16), we obtain:

$$\dot{V}_1 = \Upsilon_1^\top [\Upsilon_2 + \tau_0] = \Upsilon_1^\top \Upsilon_2 + \Upsilon_1^\top \tau_0 \quad (26)$$

By considering the description of (15), we obtain:

$$\dot{V}_1 \leq \Upsilon_1^\top \Upsilon_2 - \frac{1}{2}a_0\|\Upsilon_1\|^2 \quad (27)$$

considering (25):

$$\dot{V}_1 \leq -\beta_1 V_1 + \Upsilon_1^\top \Upsilon_2 \quad (28)$$

where $\beta_1 = a_0$. Likewise, we can establish an analogous Lyapunov function, as shown:

$$V_2 = \frac{1}{2}[\Upsilon_2^\top \Upsilon_2 + c_1^{-1}\tilde{\chi}^2] \quad (29)$$

By differentiating V_2 and inserting (16) into (29), we have:

$$\dot{V}_2 = \Upsilon_2^\top [M^{-1}\tau + F^* + \tau_d - \ddot{q}_d] + c_1^{-1}\tilde{\chi}\dot{\tilde{\chi}} \quad (30)$$

Considering (18):

$$\begin{aligned} \dot{V}_2 \leq & \Upsilon_2^\top M^{-1}\tau + \|\Upsilon_2\|mH + \|\Upsilon_2\|\tau_{\max} + \|\Upsilon_2\|A_{\max} \\ & + c_1^{-1}\tilde{\chi}\dot{\tilde{\chi}} \end{aligned} \quad (31)$$

By considering positive constants μ , v_1 , and v_2 and following Young's inequality, we have:

$$\begin{aligned} \dot{V}_2 \leq & \Upsilon_2^\top M^{-1}\tau + \frac{1}{2}\|\Upsilon_2\|^2\mu m^2 + \frac{1}{2}\|\Upsilon_2\|^2v_1\tau_{\max}^2 + \frac{1}{2}v_2^{-1} \\ & + \frac{1}{2}\mu^{-1}H^2 + \frac{1}{2}v_1^{-1} + \frac{1}{2}v_2 A_{\max}^2\|\Upsilon_2\|^2 + c_1^{-1}\tilde{\chi}\dot{\tilde{\chi}} \end{aligned} \quad (32)$$

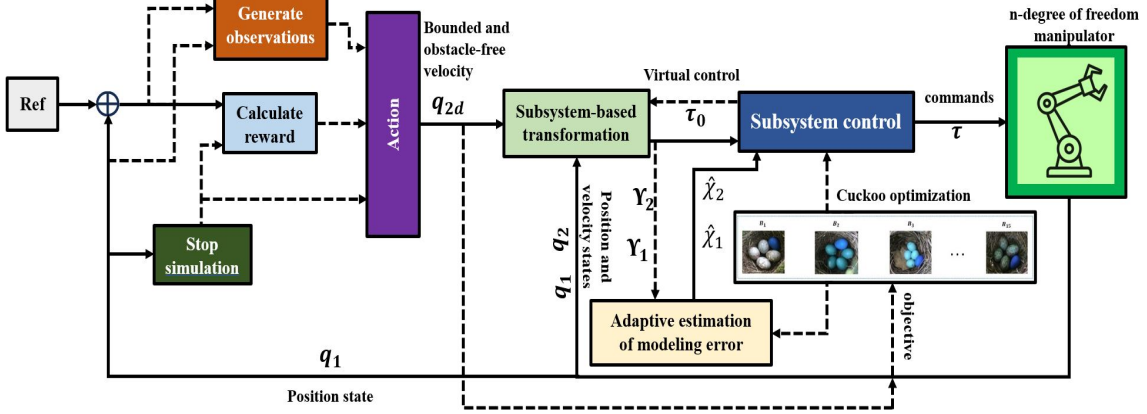


Fig. 2: Schematic of low-level robust model-free subsystem-based control and obstacle-free DRL-bounded motion planner.

Likewise, we continue by considering the control input provided in (21) and the adaptive law error provided in (23), as follows:

$$\begin{aligned} \dot{V}_2 &\leq -\frac{1}{2}a_1\|\Upsilon_2\|^2 - \frac{1}{2}b_1\hat{\chi}\|\Upsilon_2\|^2 - \Upsilon_2^\top\Upsilon_2 + \frac{1}{2}\|\Upsilon_2\|^2\mu m^2 \\ &\quad + \frac{1}{2}\|\Upsilon_2\|^2v_1\tau_{max}^2 + \frac{1}{2}v_1^{-1} + \frac{1}{2}v_2A_{max}^2\|\Upsilon_2\|^2 \\ &\quad + \frac{1}{2}\mu^{-1}H^2 + \frac{1}{2}v_2^{-1} - r_1\tilde{\chi}^2 + \frac{1}{2}b_1\|\Upsilon_2\|^2\tilde{\chi} - r_1\chi^*\tilde{\chi} \end{aligned} \quad (33)$$

Regarding (24), and knowing that $\tilde{\chi} = \hat{\chi} - \chi^*$:

$$\begin{aligned} \dot{V}_2 &\leq -\frac{1}{2}a_1\|\Upsilon_2\|^2 - \Upsilon_2^\top\Upsilon_2 + \frac{1}{2}\mu^{-1}H^2 + \frac{1}{2}v_1^{-1} + \frac{1}{2}v_2^{-1} \\ &\quad - r_1\tilde{\chi}^2 - r_1\chi^*\tilde{\chi} \end{aligned} \quad (34)$$

After dividing $r_1\tilde{\chi}^2$ into $\frac{1}{2}r_1\tilde{\chi}^2 + \frac{1}{2}r_1\tilde{\chi}^2$, we can obtain:

$$\begin{aligned} \dot{V}_2 &\leq -\frac{1}{2}a_1\|\Upsilon_2\|^2 - \Upsilon_2^\top\Upsilon_2 + \frac{1}{2}\mu^{-1}H^2 + \frac{1}{2}v_1^{-1} + \frac{1}{2}v_2^{-1} \\ &\quad - \frac{1}{2}r_1\tilde{\chi}^2 + \frac{1}{2}r_1\chi^*\tilde{\chi} \\ &\leq -\beta_2V_2 - \Upsilon_2^\top\Upsilon_2 + \frac{1}{2}\mu^{-1}H^2 + \frac{1}{2}v_1^{-1} + \frac{1}{2}v_2^{-1} + \frac{1}{2}r_1\chi^*\tilde{\chi} \end{aligned} \quad (35)$$

where $\beta_2 = \min[a_1, c_1r_1]$. Now, we can establish the Lyapunov function for the entire system, by considering the subsystem-based Lyapunov functions provided in (25) and (29), as follows:

$$V = V_1 + V_2 \quad (36)$$

After the derivative, and after inserting (28), and (35), we obtain:

$$\dot{V} \leq -\sum_{i=1}^2\beta_iV_i + \frac{1}{2}\mu^{-1}H^2 + \frac{1}{2}\sum_{i=1}^2v_i^{-1} + \frac{1}{2}r_1\chi^*\tilde{\chi} \quad (37)$$

To simplify (37), we can say:

$$\dot{V} \leq -\beta_{min}V + \frac{1}{2}\mu^{-1}H^2 + \beta^*, \quad (38)$$

where:

$$\beta_{min} = \min[\beta_1, \beta_2], \quad \beta^* = \frac{1}{2}r_1\chi^*\tilde{\chi} \quad (39)$$

Thus, regarding (39), based on the stability concept defined in [36] and on the Definition 1, Theorem 1 is proved.

V. NUMERICAL EVALUATION

To investigate the effectiveness of the methodology, we applied the proposed control strategy to the 2-DoF vertical plane robot expressed in [26] with link lengths 1m and 0.8m. As mentioned in Section III, both the controller and the manipulator model collectively form our environment. This implies the actions generated by the agent enter a closed loop encompassing both the controller and the model. Following this, environment parameters are configured (refer to Table I). Simulation resets and the beginning of a new episode occurs in instances in which a joint surpasses its limits, the manipulator attains the goal, a collision occurs, or the number of simulation steps exceeds the limit. Next, the SAC parameters are configured as outlined in Table II. The policy runs at a 33.33-Hz frequency and the controller runs at 1 KHz in the simulation.

TABLE I: DRL environment parameters.

Parameters	Value
Reach Reward	200
Boundary Penalty	50
Collision Penalty	100
Joint Limits (rad)	$q_1(1) : [-\pi/4, 3\pi/4], q_1(2) : [-5\pi/6, 5\pi/6]$
Reach Threshold (m)	0.04

TABLE II: DRL agent parameters.

Parameters	Value
Velocity Bounds (rad/s)	$q_2(1) : [-0.1, +0.1], q_2(2) : [-0.4, +0.4]$
Batch size	512
Target smoothing factor	0.001
Experience buffer length	1000000
Initial random steps	1000
Discount factor	0.995
Training episodes	20000
Time step	0.03
Max time steps/episode	1000
Learning rate	0.001

The representation of the unidentified friction and external load effects are expressed in the following manner:

$$F + \tau_d = \begin{bmatrix} 0.5 \cos(0.7q_1(2)) + 3 \cos(2r) \\ -1.1 \cos(1.8q_1(2)) + 1.8 \cos(0.3\dot{q}_1(1)) - 0.2 \end{bmatrix} \quad (40)$$

The parameters associated with CSO are considered as follows: $\zeta = 8$, $\beta = 1.5$, $n_{\text{iteration}} = 200$, $P_a = 25\%$, and $\eta = 15$. This simulation considers five different tip obstacles, the same initial conditions, and four random targets in task space, as shown in Fig. 3.

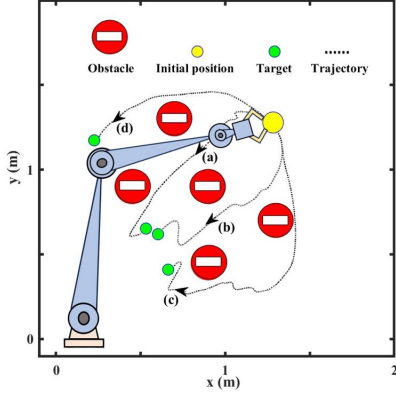


Fig. 3: Obstacle-free trajectories executed by the manipulator's tip for randomly non-repetitive tasks.

The control process ceased when the error between the tip of the robot and the target met the condition of having an error of less than 4 cm, as shown in Fig 4. The figure illustrates the target error from the initial to the target position in task space for the four different tasks. Although target (d) is the second farthest in comparison to the other targets, the task's goal was achieved the soonest in contrast to task (b), suggesting that the path involved lower complexity and fewer obstacles, leading to a quicker accomplishment.

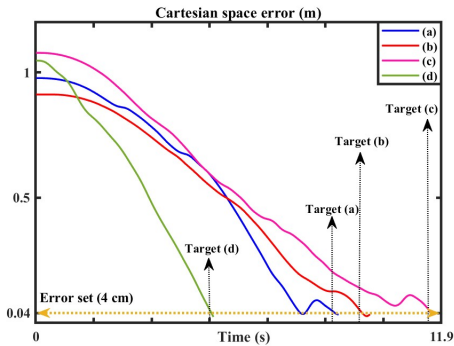


Fig. 4: The target error in task space by employing the proposed control.

In summary, the performance of the proposed control strategy is indicated in Table III. It shows that the robot system took the least amount of time (about 5.5sec) to reach the target in task (d), while task (c) required the most time (more than 11sec). In addition, tasks (a) and (c) experienced the highest torque amplitudes (400Nm), while task (d) had the least torque effort (220Nm) in reaching the target, as shown in Fig. 5. The figure illustrates that tasks involve more changes in direction necessitating higher torque generation.

TABLE III: Performance of the proposed control.

Goal-reaching tasks	Target time (s)	Target error (cm)	tracking error (cm)	Max. torque amplitude (N.m)	optimization time (s)
(a)	9.176	0.025	0.0006	400	0.01
(b)	9.92	0.037	0.0008	360	0.03
(c)	11.16	0.029	0.001	400	0.05
(d)	5.456	0.039	0.0002	220	0.009

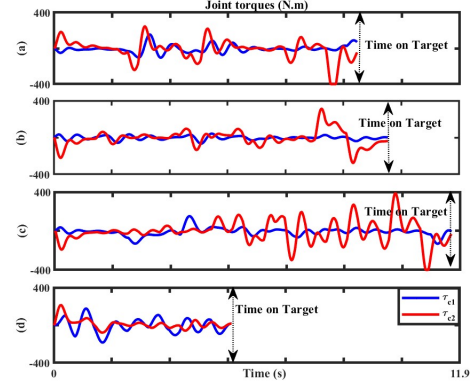


Fig. 5: Torques generated by joints to perform control targets.

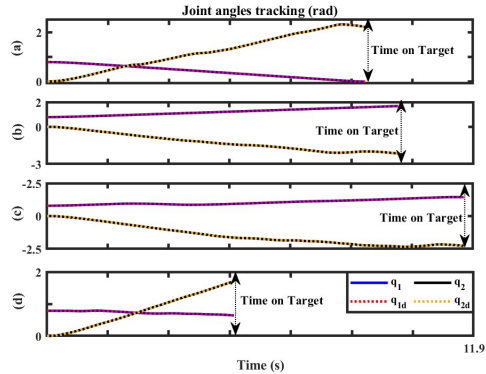


Fig. 6: Tracking of the DRL-generated trajectories by employing the proposed low-level control.

After utilizing CSO, the controller gains converged to the following values: $a_0 = 668$, $a_1 = 552$, $b_1 = 1.8$, $c_1 = 0.001$, and $r_1 = 0.69$. The performance of the tracking position and velocity references is depicted in Fig. 6, where all states converge rapidly to the respective references before 0.05 seconds when control gains are optimized. Our investigation into the same condition and for the nonrepetitive tasks to goal achievement revealed that the implementation of the proposed SAC motion planning and a low-level model-free control strategy can enhance the computational efficiency of the learning process. The proposed low-level control is not only model-free and lacks information about the environment but is also more robust, and capable of compensating for uncertainties introduced by the environment and the combination of DRL and low-level control. Our comparisons validated the improvement of speed convergence and computations, which is approximately 10% and 18% faster than the control strategies suggested in [37] and [19], respectively, while maintaining accuracy comparable.

VI. CONCLUSION

To enhance the control performance of goal-reaching tasks for a manipulator with n-DoF, this paper proposed a novel, robust low- and joint-level control strategy in velocity-bounded, obstacle-free, and non-repetitive motion planning. Hence, a model-free DRL network was provided to plan goal achievement motions with the presence of random obstacles for any initial and target points, being fed to a low-level robust subsystem-based adaptive strategy to generate sufficient joint torques, ensuring exponential convergence of tracking errors to zero in the presence of unknown uncertainties, and time-variant external disturbances. In addition, gains have been optimized using a CSO tailored to minimize the rise time, settling time, maximum overshoot, and steady-state tracking error, all while actively engaging in the learning phase through interactions with the environment.

REFERENCES

- [1] Z. Liu, Q. Liu, W. Xu, L. Wang, and Z. Zhou, "Robot learning towards smart robotic manufacturing: A review," *Robot. Comput. Integrat. Manuf.*, vol. 77, p. 102360, 2022.
- [2] M. Elbanhawi and M. Simic, "Sampling-based robot motion planning: A review," *IEEE Access*, vol. 2, pp. 56–77, 2014.
- [3] O. Kroemer, S. Niekum, and G. Konidaris, "A review of robot learning for manipulation: Challenges, representations, and algorithms," *The Journal of Machine Learning Research*, vol. 22, no. 1, pp. 1395–1476, 2021.
- [4] A. Mueller, "Modern robotics: Mechanics, planning, and control [bookshelf]," *IEEE Control Systems Magazine*, vol. 39, no. 6, pp. 100–102, 2019.
- [5] S. Karaman and E. Frazzoli, "Sampling-based algorithms for optimal motion planning," *Int. J. Robot. Res.*, vol. 30, no. 7, pp. 846–894, 2011.
- [6] M. Mukadam, J. Dong, X. Yan, F. Dellaert, and B. Boots, "Continuous-time gaussian process motion planning via probabilistic inference," *The International Journal of Robotics Research*, vol. 37, no. 11, pp. 1319–1340, 2018.
- [7] K. Hauser and V. Ng-Thow-Hing, "Fast smoothing of manipulator trajectories using optimal bounded-acceleration shortcuts," in *IEEE ICRA*, 2010, pp. 2493–2498.
- [8] J. Uraint, A. T. Le, A. Lambert, G. Chalvatzaki, B. Boots, and J. Peters, "Learning implicit priors for motion optimization," in *IEEE/RSJ International Conference on Intelligent Robots and Systems (IROS)*, 2022, pp. 7672–7679.
- [9] J. Carvalho, A. T. Le, M. Baierl, D. Koert, and J. Peters, "Motion planning diffusion: Learning and planning of robot motions with diffusion models," in *2023 IEEE/RSJ International Conference on Intelligent Robots and Systems (IROS)*, 2023, pp. 1916–1923.
- [10] M. G. Tamizi, M. Yaghoubi, and H. Najarian, "A review of recent trend in motion planning of industrial robots," *International Journal of Intelligent Robotics and Applications*, pp. 1–22, 2023.
- [11] R. S. Sutton and A. G. Barto, *Reinforcement Learning: An Introduction*. Cambridge, MA: A Bradford Book, 2018.
- [12] A. del Real Torres, D. S. Andreiana, Á. Ojeda Roldán, A. Hernández Bustos, and L. E. Acevedo Galicia, "A review of deep reinforcement learning approaches for smart manufacturing in industry 4.0 and 5.0 framework," *Applied Sciences*, vol. 12, no. 23, p. 12377, 2022.
- [13] T. Qiu and Y. Cheng, "Applications and challenges of deep reinforcement learning in multi-robot path planning," *Journal of Electronic Research and Application*, vol. 5, no. 6, pp. 25–29, 2021.
- [14] R. Liu, F. Nageotte, P. Zanne, M. de Mathelin, and B. Dresp-Langley, "Deep reinforcement learning for the control of robotic manipulation: a focussed mini-review," *Robotics*, vol. 10, no. 1, p. 22, 2021.
- [15] E. Prianto, J.-H. Park, J.-H. Bae, and J.-S. Kim, "Deep reinforcement learning-based path planning for multi-arm manipulators with periodically moving obstacles," *Applied Sciences*, vol. 11, no. 6, p. 2587, 2021.
- [16] N. Rudin, D. Hoeller, P. Reist, and M. Hutter, "Learning to walk in minutes using massively parallel deep reinforcement learning," in *Conference on Robot Learning*. PMLR, 2022, pp. 91–100.
- [17] R. Martín-Martín, M. A. Lee, R. Gardner, S. Savarese, J. Bohg, and A. Garg, "Variable impedance control in end-effector space: An action space for reinforcement learning in contact-rich tasks," in *2019 IEEE/RSJ International Conference on Intelligent Robots and Systems (IROS)*, 2019, pp. 1010–1017.
- [18] N. Wahlström, T. B. Schön, and M. P. Deisenroth, "From pixels to torques: Policy learning with deep dynamical models," *arXiv preprint arXiv:1502.02251*, 2015.
- [19] Lillicrap *et al.*, "Continuous control with deep reinforcement learning," *arXiv preprint arXiv:1509.02971*, 2015.
- [20] E. Aljalbout, F. Frank, M. Karl, and P. van der Smagt, "On the role of the action space in robot manipulation learning and sim-to-real transfer," *arXiv preprint arXiv:2312.03673*, 2023.
- [21] Y. Shan, B. Zheng, L. Chen, L. Chen, and D. Chen, "A reinforcement learning-based adaptive path tracking approach for autonomous driving," *IEEE Transactions on Vehicular Technology*, vol. 69, no. 10, pp. 10581–10595, 2020.
- [22] X.-S. Yang, *Cuckoo search and firefly algorithm: theory and applications*. Springer, 2013, vol. 516.
- [23] X.-S. Yang and S. Deb, "Cuckoo search via lévy flights," in *2009 World congress on nature & biologically inspired computing (NaBIC)*. Ieee, 2009, pp. 210–214.
- [24] A. Abdelaziz and E. S. Ali, "Cuckoo search algorithm based load frequency controller design for nonlinear interconnected power system," *International Journal of Electrical Power & Energy Systems*, vol. 73, pp. 632–643, 2015.
- [25] Z. Bingul and O. Karahan, "A novel performance criterion approach to optimum design of pid controller using cuckoo search algorithm for avr system," *Journal of the Franklin Institute*, vol. 355, no. 13, pp. 5534–5559, 2018.
- [26] J.-P. Humaloja, J. Koivumäki, L. Paunonen, and J. Mattila, "Decentralized observer design for virtual decomposition control," *Trans. Automat. Contr.*, vol. 67, no. 5, pp. 2529–2536, 2021.
- [27] H. R. Nohooji, "Constrained neural adaptive pid control for robot manipulators," *J. Franklin Inst.*, vol. 357, no. 7, pp. 3907–3923, 2020.
- [28] T. Haarnoja, Zhou *et al.*, "Soft actor-critic: Off-policy maximum entropy deep reinforcement learning with a stochastic actor," in *International conference on machine learning*, 2018, pp. 1861–1870.
- [29] Haarnoja *et al.*, "Soft actor-critic algorithms and applications," *arXiv preprint arXiv:1812.05905*, 2018.
- [30] L. Shao, T. Migimatsu, Q. Zhang, K. Yang, and J. Bohg, "Concept2robot: Learning manipulation concepts from instructions and human demonstrations," *The International Journal of Robotics Research*, vol. 40, no. 12–14, pp. 1419–1434, 2021.
- [31] M. A. Lee, Y. Zhu, K. Srinivasan, P. Shah, S. Savarese, L. Fei-Fei, A. Garg, and J. Bohg, "Making sense of vision and touch: Self-supervised learning of multimodal representations for contact-rich tasks," in *2019 International Conference on Robotics and Automation (ICRA)*, 2019, pp. 8943–8950.
- [32] V. Kumar, D. Hoeller, B. Sundaralingam, J. Tremblay, and S. Birchfield, "Joint space control via deep reinforcement learning," in *2021 IEEE/RSJ International Conference on Intelligent Robots and Systems (IROS)*, 2021, pp. 3619–3626.
- [33] A. H. Gandomi, X.-S. Yang, and A. H. Alavi, "Cuckoo search algorithm: a metaheuristic approach to solve structural optimization problems," *Engineering with computers*, vol. 29, pp. 17–35, 2013.
- [34] V. Kumar, P. Gaur, and A. Mittal, "Ann-based self-tuned pid-like adaptive controller design for high-performance pmsm position control," *Expert Systems with Applications*, vol. 41, no. 17, pp. 7995–8002, 2014.
- [35] X.-S. Yang and S. Deb, "Engineering optimisation by cuckoo search," *International Journal of Mathematical Modelling and Numerical Optimisation*, vol. 1, no. 4, pp. 330–343, 2010.
- [36] M. Heydari Shahna, M. Bahari, and J. Mattila, "Robust decomposed system control for an electro-mechanical linear actuator mechanism under input constraints," *International Journal of Robust and Nonlinear Control*, 2024.
- [37] Z. Yang, K. E. Merrick, H. A. Abbass, and L. Jin, "Multi-task deep reinforcement learning for continuous action control," in *IJCAI*, vol. 17, 2017, pp. 3301–3307.